# High surface area, low-weight composite nickel fiber electrodes

Bradley A. Johnson, Richard E. Ferro, Greg M. Swain and Bruce T. Tatarchuk
*Department of Chemical Engineering and Space Power Institute, Auburn University, Auburn, AL 36849 (USA)*

**Abstract**

The energy density and power density of lightweight aerospace batteries utilizing the nickel oxide electrode are often limited by the microstructures of both the collector and the resulting active deposit in/on the collector. Heretofore, these two microstructures have been intimately linked to one another by the materials used to prepare the collector grid as well as the methods and conditions used to deposit the active material. Significant weight and performance advantages have been demonstrated by Britton and Reid at NASA–LeRC using FIBREX nickel mats of ~28–32 μm diameter. Work in our laboratory has investigated the potential performance advantages offered by nickel fiber composite electrodes containing a mixture of fibers as small as 2 μm diameter (available from Memtec America Corporation). These electrode collectors possess in excess of an order of magnitude more surface area per gram of collector than FIBREX nickel. The increase in surface area of the collector roughly translates into an order of magnitude thinner layer of active material. Performance data and advantages of these thin layer structures will be presented. Attributes and limitations of their electrode microstructure to independently control void volume, pore structure of the $Ni(OH)_2$ deposition, and resulting electrical properties will be discussed.

## Introduction

The secondary nickel/hydrogen ($Ni/H_2$) battery is a hybrid of the secondary Ni–Cd battery and the $H_2/O_2$ fuel cell; a combination of the two best performing electrodes from these two systems. The $Ni/H_2$ battery possesses many advantages over other battery systems which include: (i) long cycle life; (ii) stability to overcharge, and (iii) a built-in state-of-charge indicator (cell pressure). However, the energy density and power density of lightweight aerospace batteries utilizing the nickel hydroxide electrode are often limited because they must be designed with large void volumes to avoid clogging of the conductive pathways with precipitant during electrochemical impregnation.

Previous research has concentrated on increasing the porosity of powder sinters while attempting to maintain acceptable structural integrity and electrical conductivity. Other attempts have been to impregnate the powder sinter substrate more efficiently with active material resulting in an increase of the electrochemical utilization. More recently, work has involved the impregnation of FIBREX (™National Standards) nickel fibers which has been shown to possess superior performance characteristics, especially in terms of weight savings compared with plaque-based materials [1]. Our laboratory has investigated the potential performance advantages offered by nickel fiber composite


*SSDI* 0378-7753(93)01768-D

electrodes [2, 3] using nickel fibers as small as 2 $\mu$m. The supposition was that the incorporation of small diameter nickel fibers (2 $\mu$m) into FIBREX, or the use of the stand-alone small diameter fiber composite electrode, would result in a significant increase in the surface area available for deposition of the active material without a significant reduction in void volume. Superior performance characteristics of the nickel fiber composite electrode have been demonstrated. By controlling the microstructure of both the collecting grid and the active deposit, the performance of the traditional nickel hydroxide electrode has been enhanced. Furthermore, the electrochemical impregnation at a reduced effective current density results in a much thinner layer of active material, which is more electrochemically accessible.

The key advantages of using small nickel fibers versus sintered nickel plaques or FIBREX include an order of magnitude higher specific surface area per gram of fiber. This not only provides increased area for the active deposit, but also increases electrochemical accessibility to the active material. Additionally, there is a low ohmic resistance within the microstructure due to the sinter bonded fibers and low mass-transport resistance within the microstructure voids resulting in easier transport of electrolytes. Moreover, this electrode can be prepared with adjustable porosities and void volumes to enhance inter- and intra-electrode transport while accommodating the required precipitation of chemical products at the cathode. Finally, its electronic properties are independent of any mechanical pressing.

## Experimental

*Electrode structure and preparation*

Sintered fiber mats were produced using small nickel fibers and cellulose. The nickel fibers had diameters of $\backsim 2$ $\mu$m and were 2 to 3 mm in length. The cellulose, a mixture of soft and hardwoods, was 20 to 30 $\mu$m in diameter and 100 to 1000 $\mu$m in length. These materials were then incorporated into a paper preform. This was done by first thoroughly mixing the metal fibers in an industrial blender. They were then agitated with the cellulose fibers until all fibers were uniformly dispersed. The solution of dispersed fibers was then further diluted and formed into a 16 cm diameter paper preform on a sheet mold. The preform was then pressed and allowed to dry in air.

Once the paper preforms were fabricated, circular discs $\backsim 19$ mm were cut from the preforms. Four of these discs were pressed together and placed on top of a 1 mil (0.025 mm) thick thin foil. This structure was then sintered at 1323 K for 30 min under a hydrogen atmosphere. The sintering creates many intimate electrical contacts per fiber and provides the mechanical stability required to withstand stress associated with swelling and contraction of the active material during cycling. Additionally, during the sintering process, virtually all of the cellulose gasifies resulting in large pores and voids inside the electrode microstructure.

The electrochemical impregnation of the $Ni(OH)_2$ active material was carried out using the methods described by Britton [1]. The electrode was placed in an acidic solution of 1.5 M $Ni(NO_3)_2$, 0.175 M $Co(NO_3)_2$, and 0.075 M $NaNO_3$. Using current densities in the range of 5–10 mA/cm$^2$ of geometrical surface area for 6 to 9 h, a loading of 1.6 g $Ni(OH)_2$/cm$^3$ was achieved. The electrochemical reduction of nitrate produces hydroxide ions in the vicinity of the bare metal fibers. Nickelous ions in solution combine with the hydroxide ions to form nickel hydroxide, which precipitates out of solution onto the surface of the fibrous network. After impregnation, the

structure is rinsed with distilled water, dried in an oven at 393 K for 1 h, and stored under ambient conditions for a minimum of 12 h.

*Electrode evaluation*

Cycle-life testing was performed in a half-cell arrangement as described by Britton [1]. A platinum gauze counter electrode was used and all potentials are reported versus a saturated calomel electrode (SCE). All measurements were made at room temperature in 26% wt.% KOH. Cyclic voltammetry and cyclic chronopotentiometry were performed using a EG&G Princeton Applied Research model 273 potentiostat/galvanostat. During cyclic chronopotentiometry, a current of *C*/2 was used, while the discharge current varied from *C*/2 to 3*C*. The *C* rate is defined as being the theoretical rate at which all active material will be reduced in a period of 1 h. From these measurements, conditioning times, capacities, and efficiencies were determined.

Scanning electron micrographs (SEM) were obtained with a JEOL 440 microscope. Both impregnated and nonimpregnated electrodes were examined to determine the overall effects of impregnation on the electrode microstructure. Furthermore, SEM was utilized to confirm the sintering of metal contacts and to view the overall fiber distribution.

## Results and discussion

Figures 1 and 2 show SEM micrographs of the nickel fiber composite electrode before and after impregnation, respectively. In the micrograph of the bare electrode, the sintered contacts between the individual fibers along with the sizable void volume can be seen (Fig. 1). The large number of sintered joints provides high conductivity pathways and mechanical strength. The impregnated electrode possesses a relatively thin and conformal coating over the entire electrode surface (Fig. 2). The active material possesses many apparent defects and grain boundaries and exhibits regions of apparent high crystallinity. The high surface area and large void volume of the

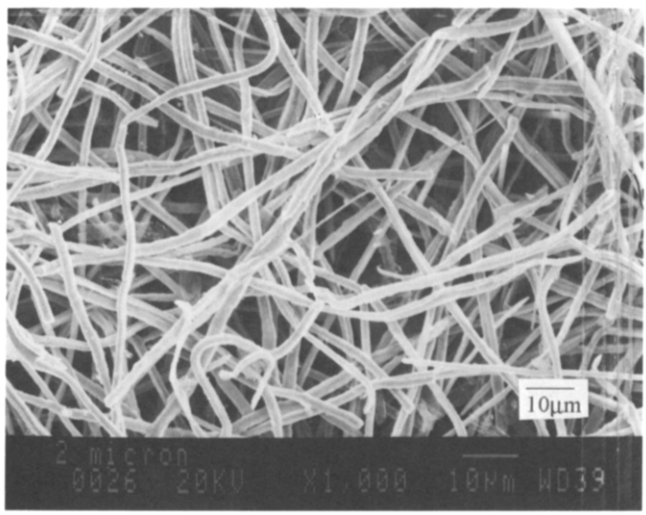


Fig. 1. SEM micrograph of a bare nickel fiber composite electrode.

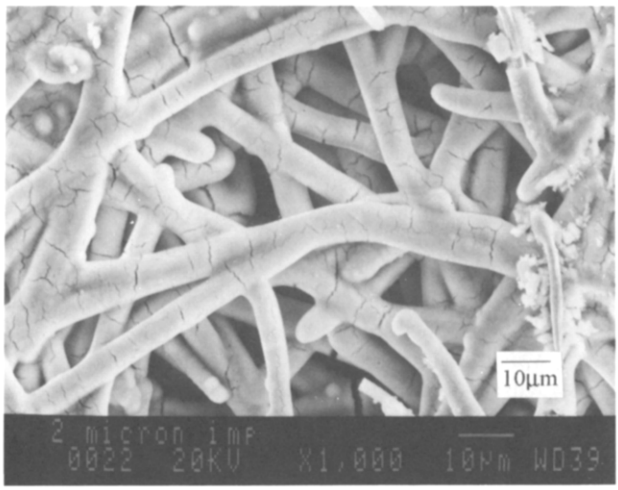


Fig. 2. SEM micrograph of an impregnated nickel fiber composite material.

electrode allows for a considerable loading of active material while maintaining a sizable void volume.

Table 1 compares the physical properties of the electrode microstructures examined during the course of this research before and after impregnation. The two columns of data most noteworthy are the values for FIBREX and those for the nickel fiber composite electrode. The composite electrode is thinner, possesses at 10-fold increase in specific surface area and is slightly more porous than FIBREX. After impregnation, the nickel fiber composite electrode possesses a higher weight of active material per unit void volume, a higher volume percent loading and a thinner layer of active material compared with FIBREX. Differences in surface area and active deposit thickness result from the smaller diameter fibers used in the composite electrode. It is important to note that, while the electrodes possessing stainless-steel fibers have a significantly larger surface area than FIBREX, the performance data were poor due to the weak adhesion of the active material to stainless steel. The incorporation of small diameter nickel fibers into FIBREX improves the physical properties of the electrode, however, the nickel fiber composite electrode possesses the most desirable properties.

Figure 3 shows typical charge and discharge curves for impregnated FIBREX and nickel composite electrodes. The loading level per unit void volume is 1.52 g/cm$^3$ and 1.69 g/cm$^3$, respectively. Again, the larger surface area of the composite electrode results in the ability to deposit a considerable amount of active material while maintaining a sizable void volume. In both cases, charging was performed at a *C*/2 rate while discharging was performed at a 3*C*/2 rate. It can be seen that the potential during charging (oxidation) at the two electrodes is $\backsim$0.8 and $\backsim$0.5 V, respectively. The more positive potential plateau at the FIBREX electrode is indicative of a higher ohmic resistance and/or mass-transport resistance and suggests that much of the current being passed is going toward oxygen evolution; a parasitic side reaction reduces the overall charge/discharge efficiency. The more negative potential plateau observed at the nickel fiber composite electrode reflects less ohmic loss and suggests that a higher percentage of the current passed is going toward the oxidation of the active material to form the oxyhydroxide rather than toward oxygen evolution, although it is likely that even all this potential oxygen evolution is occurring to some degree. Upon reversal of the

TABLE 1

Physical properties of fiber-based electrode microstructures before and after impregnation

| | FIBREX | FIBREX/ stainless steel | FIBREX/ nickel | Steel | Nickel |
|---|---|---|---|---|---|
| (a) Before impregnation | | | | | |
| Thickness (mils) | 35 | 35 | 35 | 19 | 19 |
| Surface area/ weight ($cm^2/g$) | 160.5 | 292.8 | 276.7 | 2535 | 2297 |
| Density ($g/cm^3$) | 0.49 | 0.55 | 0.55 | 0.33 | 0.35 |
| Porosity (%) | 94.4 | 93.7 | 93.7 | 95.8 | 95.8 |
| (b) After impregnation | | | | | |
| Weight of $Ni(OH)_2$ ($g/cm^3$ of void) | 0.42 | 0.21 | 0.67 | 1.12 | 0.66 |
| Porosity (%) | 80.9 | 86.7 | 74.1 | 66.0 | 75.9 |
| Loading (vol.%) | 14.3 | 7.53 | 21.0 | 30.8 | 20.5 |
| Effective thickness of $Ni(OH)_2$ ($\mu m$) | 17.1 | 6.49 | 2.64 | 3.51 | 2.47 |

current to initiate the discharge process, it can be seen that the electrode potential of FIBREX quickly drops and plateaus at a more negative potential compared with the nickel fiber electrode. Again, this difference is likely due to the increased ohmic loss with the FIBREX electrode. The most noteworthy difference between the two electrodes is the increased capacity present at the composite electrode. The percent utilization at the composite electrode is greater than 200%. The maximum utilized capacity was usually reached within 5 to 10 cycles which compares most favorably with the greater than 200 number of cycles often required for many commercially available electrodes.

Table 2 contains the specifications used in the charge and discharge cycles. The FIBREX-containing electrodes contain a larger amount of active material and consequently, a higher rating (mAh). This active deposit is relatively thick compared with that estimated for the nickel fiber composite electrode. The increased thickness produces more mass-transport impedance and results in reduced efficiency. Most importantly, the utilization typically observed at the FIBREX electrodes, containing small metal fibers, is near 200%. However, a 300% utilization is routinely observed at the nickel

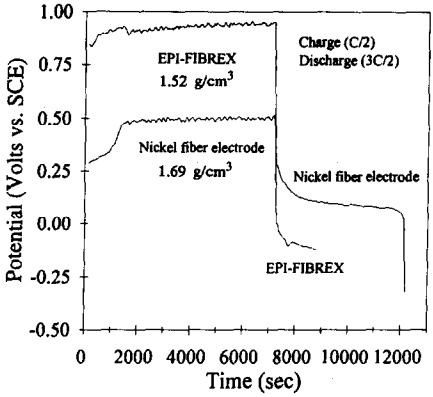


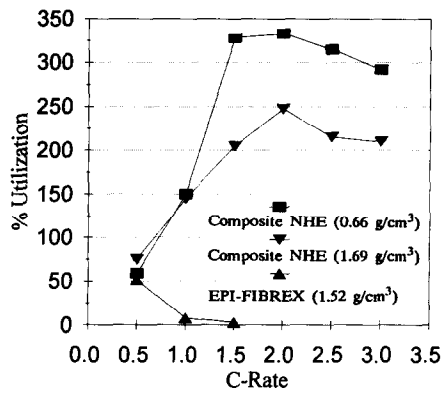


Fig. 3. Charge and discharge curves for impregnated Eagle–Picher (FIBREX-based) and nickel fiber composite electrodes in 26 wt.% KOH.

Fig. 4. Plot of percent utilization vs. discharge rate for an impregnated Eagle–Picher (FIBREX-based) and an impregnated nickel fiber composite electrode at two different loading levels in 26 wt.% KOH; charging performed at *C*/2.

fiber composite electrode. A less efficient utilization is observed at the stainless-steel composite electrode because of the poor adhesion of the active material. The active material was observed to detach from the electrode during cycling.

The effect of the discharge rate on the utilization was examined and is shown in Fig. 4. Data for a FIBREX and two nickel fiber composite electrodes are shown; one with a low loading of 0.66 g/cm$^3$ and one with a high loading of 1.69 g/cm$^3$. All charging cycles were performed at *C*/2 and each data point was obtained after 5 cycles. The data for the FIBREX electrode show the expected trend of decreasing utilization of the active material with increasing rate. This decrease is due to the deficiency of protons within the active material near the reaction sites and to the mass-transport impedance through the thick film. On the contrary, the data for the nickel fiber composite electrodes show an increasing trend of utilization with discharge rate up to a rate near 2*C* where utilization begins to decrease. Higher utilizations are observed at the composite electrode with the lower loading, as would be expected.

Figure 5 shows a plot of the percent utilization versus the cycle number for a typical impregnated composite electrode. The plot shows how the conditioning time is short at the composite electrode as full utilization is reached within the first 10 cycles. The utilization is approaching 280% after 10 cycles and remains relatively constant for the first 500 cycles. In each cycle, the charging step was performed at a *C*/2 rate and the discharging was performed at a 3*C*/2 rate. After 500 cycles, the utilization begins to decrease and by the time 1000 cycles have been performed, the utilization is near 150%. The percent utilization is defined as the ratio of the charge passed during the reduction of the active material (discharging), before the electrode potential decreases to $-0.2$ V versus SCE, to the charge passed during oxidation of the active material (charging).

Figure 6 lists some of the possible reactions which might be occurring to give rise to the anomalous increase in capacity. At present, we have not identified the source of the increased capacity but we are currently conducting a detailed mechanistic study of the nickel hydroxide/oxyhydroxide redox process at the composite electrode. One possibility involves the generation of hydrogen at the nickel electrode for extended

TABLE 2

Specifications used for the different electrode microstructures during cycle testing

| | FIBREX | FIBREX+ stainless steel | Steel | FIBREX+ nickel | Nickel |
|---|---|---|---|---|---|
| Weight (mg) | 124.6 | 138.7 | 28.70 | 185.0 | 31 |
| Weight of $Ni(OH)_2$ (mg) | 85.32 | 65.88 | 63.80 | 120.5 | 44 |
| Rating (mAh) | 24.67 | 19.04 | 18.44 | 34.84 | 12.7 |
| Charge (*C/2*) | | | | | |
| Act. Current (mA) | 12.33 | 9.52 | 9.22 | 17.42 | 6.36 |
| Time (s) | 7200 | 7200 | 7200 | 7200 | 7200 |
| Current/Weight (A/g) | 0.144 | 0.144 | 0.144 | 0.144 | 0.144 |
| Discharge (*3C/2*) | | | | | |
| Current (mA) | 35.99 | 28.56 | 27.66 | 52.26 | 19.1 |
| Time (s) | 1200 | 4800 | 1120 | 4800 | 7440 |
| Current/Weight (A/g) | 0.433 | 0.433 | 0.433 | 0.433 | 0.433 |
| Capacity (mAh) | 45.3 | 38.08 | 8.61 | 69.68 | 39.43 |
| Utilization (%) | 50 | 200 | 36.67 | 200 | 310 |

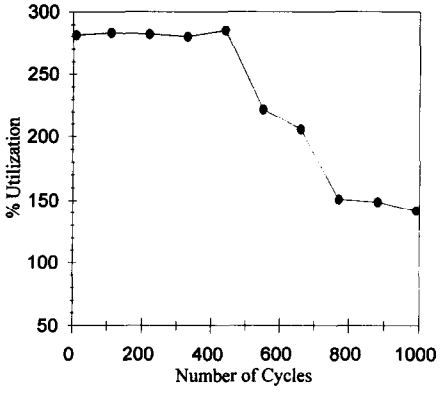


Fig. 5. Plot of the percent utilization vs. the cycle number for an impregnated nickel fiber composite electrode in 26 wt.% KOH; charging performed at *C/2* and discharging at *3C/2*.

I. Chemical Reaction:
Lower Oxide + $O_2/OH^-$ ↔ Higher Oxide

II. Growth and conditioning of active material formed on the substrate.

III. Injection of $H^+/H$ generated during HER at sites on the composite electrode into the active material.

Increased ability to discharge residual capacity by raising proton concentration which supports conductivity.

Influx of protons from remaining charged active material or from $H_2$ generated at current collector.

IV. Cycle tests performed in open atmosphere

Intercalation of anions-charge neutralization within active material.

Fig. 6. Possible reaction schemes to account for the 'anomalous' capacity observed.

periods of time during the discharge cycle. The discharge cycle tests, described herein, were always performed for a defined period of time regardless of the electrode potential value. In many cases, the electrode potential decreased to $\backsim -1.2$ V versus SCE and remains there for extended periods of time during the discharge cycle in order to maintain the desired current flow. Consequently, significant quantities of hydrogen were produced. In this same potential region, bare nickel substrate is exposed due to the reduction of nickel hydroxide. The bare substrate provides sites for the dissociative chemisorption and/or oxidation of hydrogen which can then be injected into the active material adjacent to these reaction sites. The injected protons may increase the ability to discharge residual or isolated capacity by increasing the proton concentration which supports conductivity [4]. The limiting step in the reduction of nickel oxyhydroxide to nickel hydroxide is known to be the proton transfer. Increasing the availability of protons in the active material will result in an increased utilization. The hydrogen gas generated can also be occluded within the pores and defects of the active material and react chemically with isolated nickel oxyhydroxide to reduce it back to nickel hydroxide as part of a self-discharge mechanism [5, 6].

All of the cycle tests reported herein were conducted during exposure to the atmosphere. $CO_2$ will readily dissolve in alkaline solution to form $CO_3^{2-}$ anions. These anions may affect the overall performance by intercalating and assisting in the compensation of the excess charge introduced by the presence of $CO_3^+$ and higher nickel oxides [7]. It is also possible that the $CO_3^{2-}$ anions can be reduced to a hydrocarbon species. Another possible reaction which may contribute to the charge passed during discharge is the reduction of carbon in the presence of excess protons to form methane. The carbon forms on the electrode surface because of the incomplete gasification of the cellulose during the sintering process. This is only speculation at this point as the potentials at which these two reactions occur at a substantial rate have not been identified. Additional sources for the extra capacity may also involve the chemical reaction of occluded oxygen with the lower oxide to form the higher oxide. If this reaction were to occur at an appreciable rate in competition with the electrochemical reduction during discharge, then additional capacity could be obtained. This chemical reaction may have more of an influence on the performance of the composite electrode

given the thin and conformal nature of the active material deposit. Also, oxygen reduction may occur concomitant with the reduction of the higher oxide [8]. Finally, some additional capacity will result from the oxidation of the bare nickel substrate.

**Acknowledgements**

The authors wish to thank NASA–LeRC Electrochemical Technology Branch, Contract #NAG3-1154, as well as Doris Britton, Patricia O'Donnell and Peggy Reid.

**References**

1 D.L. Britton, Lightweight fibrous nickel electrode for nickel hydrogen battery, *NASA-TM-100958,* 1988.
2 D. Kohler, J. Zabasajja, A. Krishnagopalan and B. Tatarchuk, *J. Electrochem. Soc., 137* (1990) 136.
3 D. Kohler, J. Zabasajja, F. Rose and B. Tatarchuk, *J. Electrochem. Soc., 137* (1990) 1750.
4 A.H. Zimmermann, in D.A. Corrigan and A.H. Zimmermann (eds.), *Proc. Symp. Nickel Hydroxide Electrodes, Hollywood, FL, USA, Oct. 16–18, 1989,* Vol. 90-4, The Electrochemical Society, Pennington, NJ, USA, 1990, p. 311.
5 Z. Mao and R.E. White, *J. Electrochem. Soc., 139* (1992) 1282.
6 A. Visintin, S. Srinivasan, A.J. Appleby and H.S. Lin, *J. Electrochem. Soc., 139* (1992) 985.
7 C. Delmas, Y. Borthomiell and C. Fauce, in D.A. Corrigan and A.H. Zimmermann (eds.), *Proc. Symp. Nickel Hydroxide Electrodes, Hollywood, FL, USA, Oct. 16–18, 1989,* Vol. 90-4, The Electrochemical Society, Pennington, NJ, USA, 1990, p. 119.
8 D.T. Sawyer and L.V. Interrante, *J. Electroanal. Chem., 2* (1961) 310.